PAPER Nr.: 66

ON THE DISPLACEMENT AND LOAD DETERMINATION OF A HELICOPTER ROTOR BLADE WITH AND WITHOUT HIGHER HARMONIC CONTROL

BY

LIU SHOUSHEN
NANJING UNIVERSITY OF AERONAUTICS AND ASTRONAUTICS
NANJING, CHINA

JERRY P. HIGMAN AND DANIEL P. SCHRAGE
GEORGIA INSTITUTE OF TECHNOLOGY
ATLANTA, GEORGIA, USA

TWENTIETH EUROPEAN ROTORCRAFT FORUM
OCTOBER 4 - 7, 1994 AMSTERDAM

Printed by the Technical Highschool Haarlem

On The Displacement And Load Determination Of A Helicopter Rotor Blade With And Without Higher Harmonic Control

Liu ShouShen†
Nanjing University of Aeronautics and Astronautics
Nanjing, China

Jerry P. Higman†† and Daniel P. Schrage
Georgia Institute of Technology
Atlanta, Georgia, USA

Abstract

In this paper, the displacements and loads of a helicopter rotor blade in forward flight with and without Higher Harmonic Control (HHC) are determined by an identification technique using measured bending moments from the blade. The ill-conditioned problem and the underdetermined problem are encountered, investigated, and solved. The Singular Value Decomposition (SVD) method is, for the first time, successfully applied in the rotor load determination process. A recurrence formula, in matrix form, is developed to calculate the generalized coordinates. Based on the determined results for three flight test cases, the difference of the rotor blade displacements and loads between baseline (HHC-off) and HHC-on with different lateral control excitation input phases is analyzed and the influence of HHC is shown.

Introduction

The concept of Higher Harmonic Control (HHC), since the late 1970's, has received much attention and regard as a means to significantly reduce helicopter vibrations. This fact is illustrated by the various works conducted in the areas of analytics [1] [2], wind tunnel tests [3] and flight tests [4] to [7], for example. The principal behind HHC is to alter the harmonic content of the blade's airloads in such a way as to reduce the forces at the blade root and ultimately reduce the amplitudes of the primary vibrations in the fuselage. The blade's harmonic airloads are modified by means of superimposing into the blade pitch control system an N/rev blade pitch oscillation. The N/rev oscillation amplitude and phase can be controlled by either open loop or closed loop feedback with the objective being to minimize the overall vibration at some point in the fuselage. The aforementioned works were performed with the goal of developing a successful HHC system and determining its potential in vibration reduction through testing. Great achievements have been made in the development of the HHC system, but further analysis on the test results is still needed, especially to address the influence and change in the harmonics of the rotor blade's airloads and displacements due to HHC. The accurate determination of rotor blade airloads in general is an on going effort and much work needs to be done. In view of the problems which still exist for predicting rotor loads, it is appropriate to determine the displacements and loads of the rotor blade using the identification technique and the existing flight test data. This is the motivation for the work described in this paper. Although some work has been conducted on the determination of the displacements and loads of the rotor blade [8] to [14], this identification technique is still under development and many practical problems need to be investigated and solved. For example, the ill-conditioned problem and the underdetermined problems are very important and have not been investigated in the rotor load identification before. Because of this, the practical application and improvement of the technique for rotor blade displacement and load determination are in need of investigation. Therefore, the main objectives of this paper are 1) the practical application and improvement of the technique for rotor blade displacement and load determination and 2) a comparative

---

† Currently at the Georgia Institute of Technology as a visiting professor.

†† Currently a doctoral student at the Georgia Institute of Technology on leave from the Naval Air Warfare Center, Aircraft Division, Patuxent River, MD.

Presented at the Twentieth European Rotorcraft Forum, Amsterdam, The Netherlands, October 4-7, 1994.

investigation and analysis of the alteration of the blade airloads and displacements due to HHC-on with that of HHC-off.

The SVD (Singular Value Decomposition) method, for the first time, is utilized in the helicopter rotor load determination process to solve the inverse problem and to identify possible difficulties due to the ill-conditioned problem thereby helping to insure the correct solution. The differences of the blade displacements and loads due to HHC-on and HHC-off are investigated and analyzed so that the effects of HHC on the displacements and loads of the rotor blade, based on flight tests, can be shown for the first time. For the purposes of this paper, data from a series of HHC flight tests of a light helicopter with a four bladed articulated rotor in forward flight were used. Also, since the task of analyzing the helicopter rotor loads for this project is in the initial stages and because of the limited amount of experimental data that is available, only flapwise displacements and loads of the rotor blade for two HHC-on cases and a baseline (HHC-off) case at the same forward flight condition are considered in this paper.

The Process of Rotor Blade Displacement and Load Determination

The measured data available from the HHC flight tests that were utilized in this study were the vibratory bending moments of the blade at 7 radial stations along the blade and the blade flap angle at the hinge. The data provide the time histories and magnitudes, phases and frequencies for the first 12 harmonics. The process of the determination of the rotor blade displacements and loads, based on this data, are as follows:

1) Determine the harmonic coefficients of the experimental bending moments and flap angle.

The measured bending moments $M(r_i,t)$ and flap angle $\beta(t)$ can be expressed as

$$M(r_i,t) = \sum_{k=1}^{N} (M_{kc}(r_i)\cos(k\Omega t) + M_{ks}(r_i)\sin(k\Omega t)) \quad (1)$$

$$\beta(t) = \sum_{k=1}^{N} (\beta_{kc}\cos(k\Omega t) + \beta_{ks}\sin(k\Omega t)) \quad (2)$$

where r_i is the radial coordinate of the measured station, k is the order of the harmonic, t is time, Ω is the rotor speed and N is the number of harmonics considered. Since the experimental data provide the magnitudes, phases and frequencies, it is easy to determine the harmonic component coefficients $M_{kc}(r_i)$, $M_{ks}(r_i)$ and β_{kc}, β_{ks}.

2) Determine the rotor blade's modal properties.

The rotor blade's natural frequencies ω_j, the corresponding mode shapes for the displacement $W_R^{(j)}(r)$ and bending moment $M_R^{(j)}(r)$, the slope β_j and the shear force Q_j at the flap hinge must be determined for the given rotor speed Ω.

3) Calculate the generalized coordinates.

The experimental bending moments $[M_e]$ may be expressed as

$$[M_e] = [M_R][q] \quad (3)$$

where $[M_e]$ is the experimental bending moment matrix

$$[M_e] = [\{M_{1c}(r_i)\}\{M_{1s}(r_i)\}..\{M_{Nc}(r_i)\}\{M_{Ns}(r_i)\}] \quad (4)$$

$[M_R]$ is the modal bending moment matrix

$$[M_R] = \left[\left\{M_R^{(1)}(r_i)\right\}\left\{M_R^{(2)}(r_i)\right\}..\left\{M_R^{(m)}(r_i)\right\}\right] \quad (5)$$

and [q] is the generalized coordinate matrix

$$[q] = \begin{bmatrix} q_{1c}^{(1)} & q_{1s}^{(1)} & \cdots\cdots & q_{Nc}^{(1)} & q_{Ns}^{(1)} \\ q_{1c}^{(2)} & q_{1s}^{(2)} & \cdots\cdots & q_{Nc}^{(2)} & q_{Ns}^{(2)} \\ \vdots & \vdots & \ddots\cdots & \vdots & \vdots \\ \vdots & \vdots & \cdots\ddots & \vdots & \vdots \\ \vdots & \vdots & \cdots\cdots & \ddots & \vdots \\ q_{1c}^{(m)} & q_{1s}^{(m)} & \cdots\cdots & q_{Nc}^{(m)} & q_{Ns}^{(m)} \end{bmatrix} . \quad (6)$$

In the above equations, the r_i is a particular radial station, the superscript represents the mode order, the subscripts kc and ks represent the cosine and sine components of the kth harmonic, respectively.

From the $[M_e]$ and $[M_R]$, the generalized coordinate matrix can be obtained

$$[q] = [M_R]^+ [M_e] . \quad (7)$$

4) Determine the structural loads -- bending moment distribution M(r,t).

Since the modal bending moments $M_R^{(j)}(r)$ and the generalized coordinates [q] are known, the bending moment distribution along the blade at time t can be calculated as

$$M(r,t) = \sum_{k=1}^{N} (M_{kc}(r) \cos(k\Omega t) + M_{ks}(r) \sin(k\Omega t)) \quad (8)$$

where

$$M_{kc}(r) = \sum_{j=1}^{m} M_R^{(j)}(r)\, q_{kc}^{(j)}$$
$$M_{ks}(r) = \sum_{j=1}^{m} M_R^{(j)}(r)\, q_{ks}^{(j)} \quad (9)$$

It should be noted that here, r could be the radial coordinate of any desired point along the blade and not just of the measured blade stations.

5) Determine the vertical force at the flap hinge and the hub loads.

The vertical force Q, at the flap hinge can be obtained from the generalized coordinates [q] and the modal vertical force Q_j at the flap hinge:

$$[Q] = [Q_j][q] \quad (10)$$

where

$$[Q] = [Q_{1c}\ Q_{1s}\ Q_{2c}\ Q_{2s} \cdots Q_{Nc}\ Q_{Ns}] \quad (11)$$

$$[Q_j] = [Q_1\ Q_2\ Q_3 \cdots Q_m] \quad (12)$$

The total vertical force Q at flap hinge is

$$Q(t) = \sum_{k=1}^{N} (Q_{kc} \cos(k\Omega t) + Q_{ks} \sin(k\Omega t)) \quad (13)$$

The vertical forces and pitch and roll moments at the hub can then be determined from the root vertical forces due to all of the blade.

6) Determine the displacements of the blade.

The displacement of any point along the blade at time t, W(r,t) may be calculated from the modal displacements $W_R^{(j)}(r)$ and the generalized coordinates [q]

$$W(r,t) = \sum_{k=1}^{N} (W_{kc}(r) \cos(k\Omega t) + W_{ks}(r) \sin(k\Omega t)) \quad (14)$$

where

$$W_{kc}(r) = \sum_{j=1}^{m} W_R^{(j)}(r)\, q_{kc}^{(j)}$$
$$W_{ks}(r) = \sum_{j=1}^{m} W_R^{(j)}(r)\, q_{ks}^{(j)} \quad (15)$$

7) Determine the airloads on the blade.

The distributed airloads on the blade may be expressed as

$$F(r,t) = \sum_{k=1}^{N} (F_{kc}(r) \cos(k\Omega t) + F_{ks}(r) \sin(k\Omega t)) \quad (16)$$

and the harmonic components $F_{kc}(r)$, $F_{ks}(r)$ may be expanded as a series in the mode shapes:

$$F_{kc}(r) = \sum_{j=1}^{m} m(r)\, W_R^{(j)}(r)\, f_{kc}^{(j)}$$
$$F_{ks}(r) = \sum_{j=1}^{m} m(r)\, W_R^{(j)}(r)\, f_{ks}^{(j)} \qquad (17)$$

The loading coefficients $f_{kc}^{(j)}$, $f_{ks}^{(j)}$ can be obtained from

$$f_{kc}^{(j)} = \left(\omega_j^2 - k^2\,\Omega^2\right) q_{kc}^{(j)}$$
$$f_{ks}^{(j)} = \left(\omega_j^2 - k^2\,\Omega^2\right) q_{ks}^{(j)} \qquad (18)$$

where it is assumed that the analyzed system is structurally undamped. The above procedure for blade displacement and load determination is shown in Figure 1.

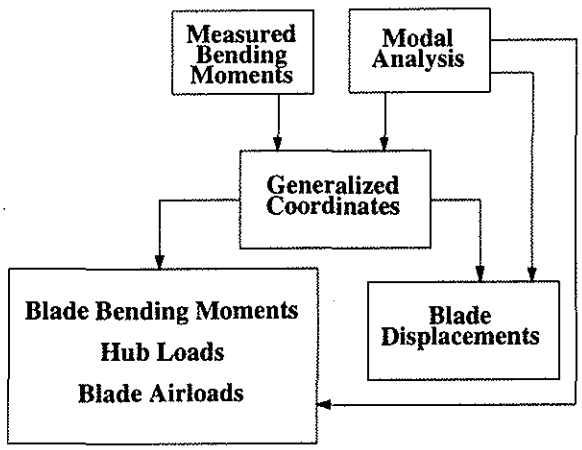

Fig. 1 Rotor blade displacement and load determination

Some Practical Problems and Approaches for the Inverse Problem

It is obvious that the calculation of the generalized coordinates [q] is the key to displacement and load determination and obtaining the generalized coordinates is an inverse problem. As in many inverse problems, in the present subject, there are two main difficult problems. One is due to ill-conditioning and another is lack of experimental data. To solve these practical problems, the SVD (Singular Value Decomposition) method, an iterative process and an approach to add some constraints are used.

1) SVD method and ill-conditioned problem.

(1) SVD method [15] and its application.

Assume [A] is an n×m matrix with n≥m (this assumption is made for convenience only). The SVD method involves factoring [A] into a product $[U][\Sigma][V]^T$, where [U] is an n×n orthogonal matrix, [V] is an m×m orthogonal matrix, and [Σ] is an n×m matrix whose off diagonal entries are all 0's and whose diagonal elements satisfy

$$\sigma_1 \geq \sigma_2 \geq \cdots \geq \sigma_m \geq 0$$

$$[\Sigma] = \begin{bmatrix} \sigma_1 & & & \\ & \sigma_2 & & 0 \\ & & \ddots & \\ & & & \sigma_m \\ & 0 & & \end{bmatrix} \qquad (19)$$

The σ_i's determined by this factorization are unique and are called the singular values of [A]. More generally, if [A] is an n×m matrix of rank r, the matrix [Σ] will be an n×m matrix of the form

$$[\Sigma] = \begin{bmatrix} \Sigma_1 & 0 \\ 0 & 0 \end{bmatrix} = \begin{bmatrix} \sigma_1 & & & & & \\ & \sigma_2 & & 0 & & \\ & & \ddots & & & \\ & & & \sigma_r & & \\ & & & & 0 & \\ & 0 & & & & \ddots \\ & & & & & & 0 \end{bmatrix} \qquad (20)$$

and the pseudo inverse of [A] is

$$[A]^+ = [V][\Sigma]^+[U]^T \qquad (21)$$

where

$$[\Sigma]^+ = \begin{bmatrix} \Sigma_1^{-1} & 0 \\ 0 & 0 \end{bmatrix} \qquad (22)$$

and

$$[\Sigma_1]^{-1} = \begin{bmatrix} \frac{1}{\sigma_1} & & 0 \\ & \frac{1}{\sigma_2} & \\ & & \ddots \\ 0 & & \frac{1}{\sigma_r} \end{bmatrix} . \qquad (23)$$

The pseudo inverse $[A]^+$ can be used in solving least squares problems. It has been proven that if [A] has a full rank, then for $[A]\{x\} = \{b\}$, the $[A]^+\{b\}$ is the least squares solution. In the case where [A] has rank r<m, there are infinitely many solutions to the least squares problem and $[A]^+\{b\}$ is the minimal solution with respect to the 2-norm.

The SVD method is suitable for the ill-conditioned problem. When the singular values $\sigma_1, \sigma_2, ..., \sigma_m$ of the n×m matrix [A] (n≥m) are known, the condition number of the matrix is very easy to calculate

$$\text{cond}(A) = \frac{\sigma_1}{\sigma_m} \qquad (24)$$

and it is an indicator of the problem condition.

For the displacement and load determination, Eq. 3 should be solved to obtain the generalized coordinate [q]. In some cases, the problem may be ill-conditioned. By using the SVD method, the singular values $\sigma_1, \sigma_2, ..., \sigma_m$ of $[M_R]$ (n×m, n≥m) first are obtained and then the condition number can be calculated. The condition number gives a measure of sensitivity of the computed [q] to errors in $[M_R]$ and $[M_e]$ (Eq. 3). If the condition number is large, small changes in $[M_R]$ or in $[M_e]$ can lead to large changes in [q]. The large condition number should result from small singular value σ_m. Using the SVD method, it is easy to find which factor leads to the small singular value so that the ill-conditioned problem could be solved. Therefore, the SVD method is suitable for calculating the pseudo inverse, $[M_R]^+$, and it is quite useful in indicating the problem condition and the source of ill-conditioning. Some ill-conditioned problems and how they are indicated by SVD will be shown in the following section.

(2) ill-conditioned problem.

In some cases, the matrix $[M_R]$ may contain some elements which lead to the ill-conditioned problem. In those cases, small variations in the input data can cause large variations in the solution. Obviously, while solving the inverse problem, it is important to explore the ill-conditioned problem. As mentioned above, the condition number is a reliable indicator of the condition, and it is easy to obtain the condition number by using SVD method. Some examples are as follows:

A. $[M_R]$ contains unsuitable mode(s).

In a test case, the modal bending moment matrix $[M_R]$ consists of the first nine modes and the number of measurement stations is 12, the pseudo-inverse $[M_R]^+$ is calculated by using the SVD method. During the calculation of $[M_R]^+$, the singular values and condition number are also obtained. For this case, the maximum (first) and minimum (last) singular values σ_1, σ_9 and the condition number are 84170.6, 0.230393 and 365335, respectively.

Given a set of experimental data $\{M_e\}$, the corresponding {q} may be obtained

$$\{q\} = [M_R]^+ \{M_e\} \qquad (25)$$

The generalized coordinate corresponding to the first mode, for the given example, is q_1= -0.351537.

The effect of errors in the measurements $\{M_e\}$ and the modal bending moments $[M_R]$ are evaluated respectively by assuming that ±5% errors are distributed randomly throughout the data. When $\{M_e\}$ has the ±5% random errors, the value of q_1 changes to -7.0244 or 1.99272 (for two tests) and when $[M_R]$ has these errors imposed, the value of q_1 changes to 6.82523. It is obvious that although there are only ± 5% random errors, the value of q can change significantly.

If $[M_R]$ is modified to consist of only the first eight modes, the maximum and minimum singular values σ_1, σ_8 and the

condition number are 65547.2, 0.282359 and 232141, respectively. For the same $\{M_e\}$ as above, the generalized coordinate is now q_1=15.0659. The difference between this result and the result from 9 modes is also too large.

But if $[M_R]$ excludes the first mode, say, $[M_R]$ consists of the modes from the 2nd through the 9th, and the measurement station is still the same 12 points, then the maximum and minimum singular values and the condition number change to 84170.6, 1408.57 and 59.756, respectively. The errors tests show that it is well conditioned. Obviously, the ill-conditioned problem of matrix $[M_R]$ which includes the first 9 modes arose from the first mode.

B. Unsuitable data points.

If there are unsuitable data points, for example, two data points which are too close in proximity, this can also lead to an ill-conditioned problem. A case is tested in which there are 9 data points and 8 modes excluding the 1st mode but 3 points are very close. The maximum singular value is 70691, the minimum is 3.68282, and the condition number is 19194.8. The error tests show large changes in the results for 5% $[M_R]$ or $[M_e]$ random change.

C. Unsuitable relationship between data points and modes.

If the relationship between data points and modes is unsuitable, the ill-conditioned problem may also arise. For example, if there are only 7 data points and $[M_R]$ consists of the 3rd to the 8th mode, even though $[M_R]$ is a 7×6 matrix (i.e. n>m) and does not include the 1st and 2nd modes, it is still ill-conditioned. The maximum and minimum singular values and the condition number are 49361.7, 322.573 and 153.025, respectively. The error test results are not satisfactory. But if for the same data points $[M_R]$ contains the 2nd to the 7th mode, then it is well conditioned. In that case, the maximum singular value is 37907.2, the minimum is 937.693, and the condition number is only 40.426.

Since the condition number and small singular value obtained from the SVD method indicate the ill-conditioned problem and the source of the problem, it is easy to solve the problem. For example, for case A, it is indicated that the first mode needs to be excluded. For case B, the data points should be changed and/or rearranged. For case C, it seems that higher modes should not be used.

For case A, another approach was tried to solve the problem. In this approach the measured flap angles at the root were used as an additional experimental data point and the modal slope at the root was appended to the bending moment modes for each mode shape. However, this approach yielded unreasonable results and it is concluded that it cannot be used to solve the ill-conditioned problem even if weighted flap angle data were used.

So to solve the problem, the first mode should be excluded. Therefore, in order to determine the generalized coordinate q_1, an iterative process is incorporated.

2) Iterative process to calculate the generalized coordinate [q].

As shown above, for this articulated rotor, if $[M_R]$ includes the first mode, the problem is ill-conditioned, but if $[M_R]$ excludes the first mode, and the data points are suitable, then it is well conditioned. So an iterative process [10] is used to calculate the generalized coordinate. The recurrence formula is developed as follows:

For the first step, the generalized coordinates of the first mode for all of the harmonic components kc, ks is

$$\left\{q_{1,k}^{(1)}\right\} = \frac{1}{\beta_1}\left\{\beta_{e,k}\right\} \tag{26}$$

and for the (n+1) step, which is based on $\left\{q_{1,k}^{(n)}\right\}$,

$$\left\{q_{1,k}^{(n+1)}\right\} = \frac{1}{\beta_1}\left(\left\{\beta_{e,k}\right\} - \left[[M_{R,j}]^+\left([M_{e,k}] - \{M_1\}\left\{q_{1,k}^{(n)}\right\}^T\right)\right]^T\{\beta_j\}\right) \tag{27}$$

where n=1,2,3, ...

The vector $\{q_{1,k}\}$ is iterated until its change is less than a given tolerance, say,

10^{-6} and then used to calculate the other generalized coordinates

$$[q_{j,k}] = [M_{R,j}]^{+} \left([M_{e,k}] - \{M_1\} \left\{ q_{1,k}^{(n+1)} \right\}^T \right). \quad (28)$$

In the above formula the generalized coordinate is,

$$\{q_{1,k}\} = \left[q_{1c}^{(1)} \; q_{1s}^{(1)} \; q_{2c}^{(1)} \; q_{2s}^{(1)} \cdots q_{Nc}^{(1)} \; q_{Ns}^{(1)} \right]^T \quad (29)$$

and

$$[q_{j,k}] = \begin{bmatrix} q_{1c}^{(2)} & q_{1s}^{(2)} & \cdots\cdots & q_{Nc}^{(2)} & q_{Ns}^{(2)} \\ q_{1c}^{(3)} & q_{1s}^{(3)} & \cdots\cdots & q_{Nc}^{(3)} & q_{Ns}^{(3)} \\ \vdots & \vdots & \ddots & \vdots & \vdots \\ \vdots & \vdots & \cdots\ddots & \vdots & \vdots \\ \vdots & \vdots & \cdots\cdots & \ddots & \vdots \\ q_{1c}^{(m)} & q_{1s}^{(m)} & \cdots\cdots & q_{Nc}^{(m)} & q_{Ns}^{(m)} \end{bmatrix}. \quad (30)$$

β_1 is the slope of the first modal displacement at the flap hinge and

$$\{\beta_j\} = \left[\beta_2 \; \beta_3 \cdots \beta_m \right]^T \quad (31)$$

are the slopes of the 2nd to mth modal displacements at the flap hinge.

$$\{\beta_{e,k}\} = \left[\beta_{e,1c} \; \beta_{e,1s} \; \beta_{e,2c} \; \beta_{e,2s} \cdots \beta_{e,Nc} \; \beta_{e,Ns} \right]^T \quad (32)$$

are the experimental root flapping angles for all of harmonic components. The vectors and matrices are defined below.

$\{M_1\}$ is the first modal bending moment vector.

$[M_{R,j}]$ is the modal bending moment matrix and only consists of the 2nd to the mth modes.

$[M_{e,k}]$ is the experimental bending moment matrix as $[M_e]$ in the Eq. 3.

The quantities n, m, N are the number of iteration, modal modes and the harmonics, respectively.

The superscript "T" represents the transpose and "+" represents the pseudo-inverse.

It is important to note that the matrix $[M_{R,j}]$ in the iterative process has to be well conditioned.

3) <u>The Overdetermined and Underdetermined Problems.</u>

For Eq. 3,

$$\underset{nxm}{[M_e]} = [M_R][q] \quad (33)$$

if $[M_e]$ is a square matrix (n=m) and nonsingular, it can easily be inverted to obtain

$$[q] = [M_R]^{-1} [M_e] \quad (34)$$

In this case, the number of experimental data, n equals the number of unknown generalized coordinates, m. The information is just sufficient to uniquely determine all of the unknowns. If there are more data than unknowns (n>m), then the problem is overdetermined. This case is often desirable because it could achieve averaging of random errors in the data. On the contrary, if there are more unknowns than data (n<m), the problem is underdetermined and difficulty arises to obtain a reasonable solution. This problem is undesirable and should be avoided if possible.

For the overdetermined problem, the solution can be obtained in terms of the pseudo-inverse, $[M_R]^+$, as described before,

$$[q] = [M_R]^{+} [M_e] \quad (35)$$

and the SVD method can be used to calculate $[M_R]^+$. In this case, because n>m (more data than unknowns), it is impossible to get a set of unknowns which will satisfy the data exactly. The idea is to select a matrix [q] such that the calculated [M] from Eq. 3 could fit the measured moment $[M_e]$ according to some minimization logic such as least-squares.

For the underdetermined problem, the solution can also be obtained by the SVD method. The form is the same as the overdetermined problem, but in this case, because n<m, there is insufficient information for a unique determination of all the unknowns. The results obtained using the SVD method is a set of solutions with a

minimum norm. Unfortunately, this solution generally gives very poor results.

In this analysis, there are only 7 experimental data points. It was found after investigation that to obtain reasonable results for some harmonics, $[M_R]$ should consist of more than 7 modes. Consequently, the underdetermined problem arose.

A number of numerical experiments and investigation were conducted and the following conclusions were drawn:

(1) For some of the harmonic components of the measured moments, the moment distribution along the radius of the blade should be fitted using more than 7 modes and the first 9 modes are desirable.

(2) If only 7 data points are used, the modes used to fit the data should only consist of the first 7 or less, otherwise, the underdetermined problem or ill-conditioned problem can arise and the results will probably not be correct.

(3) The best way to solve the underdetermined problem is to avoid the problem. To obtain reasonable results, it seems that more than 9 measured data points for flapwise load identification is desirable.

(4) If an underdetermined problem has to be treated, a reasonable solution can only be obtained by adding some constraints to the problem. It is obvious that the solution will not be unique because of the number of different constraints that could be used. In this case, experience and engineering judgment are very important.

In this paper, in order to use the first 9 modes, 3 points were added to the experimental points, allowing an underdetermined problem (n=7, m=9) to become an overdetermined problem (n=10, m=9). The data for the 3 points were generated by interpolating the experimental data. The resulting interpolation curve is determined by using some constraints such as the force boundary conditions, etc.

4) Analysis and Check.

In order to analyze and check the results of the load identification methodology, a predicted response analysis is conducted by using the determined loads. The flapwise bending moments can be obtained and are compared with the experimental data. The Force Integration Method is used for the bending moment calculation. Using this method as a check, it is quite easy and useful in the analysis to examine the contributions of individual terms - aerodynamic loads, inertial forces and centrifugal forces.

Results and Discussion

After solving the ill-conditioned and underdetermined problems, the displacements and loads of the light helicopter rotor blade are determined following the process described above. Experimental data with the helicopter at 60 knot level flight condition during the open loop HHC phase of the flight test program were used. In support of the main objectives stated in the introduction, the following three flight test cases were analyzed: HHC-off (baseline case), HHC-on with excitation input phase at 120 deg. and HHC-on with excitation input phase at 330 deg. The excitation input for both HHC-on cases were due to a 4/rev lateral cyclic control input which produced about $\pm$ .3 deg. of blade pitch oscillation. The work, described in the paper, arrived at the results of the determined vibratory distributed displacements, bending moments, shear forces and airloads on the blade. Some of the results of this analysis are presented below. Also presented are the results from the predicted response analysis due to the determined airloads which are presented for check and verification.

Figures 2(a), (b) and (c) show the blade flap bending moment time history at r/R=0.7, HHC-off, HHC-on 120 deg. and HHC-on 330 deg. cases, respectively. In these figures are shown the experimental data and the response analysis results using the determined airloads from the corresponding case. Good agreement between them can be observed. This is only a sample of the results considered and for all of the cases analyzed the conclusions are the same.

Figures 3(a), (b) and (c) show the 3rd, 4th and 5th harmonic components of the bending moments distributed along the radius of the blade, respectively. The dots represent the experimental data and the lines represent the results determined by the identification technique and calculated from the response analysis by using the determined airloads. Both of the determined and calculated bending moments compare very well. It can

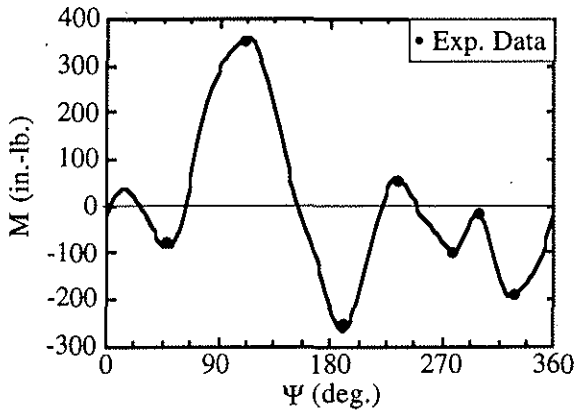

2(a) HHC-off

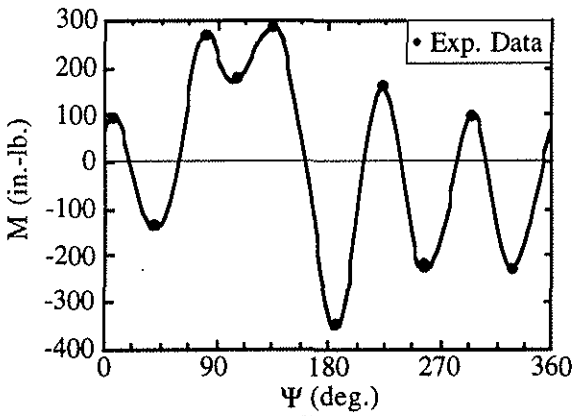

2(b) HHC-on 120 deg.

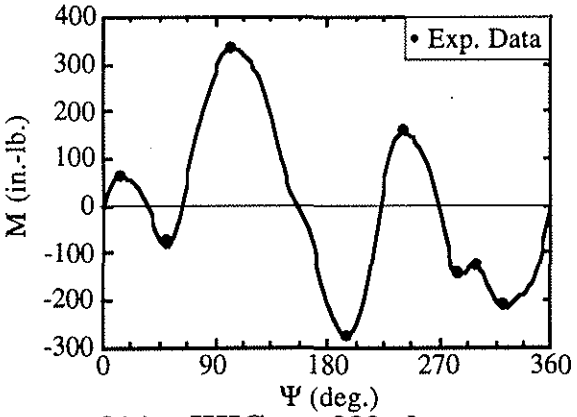

2(c) HHC-on 330 deg.

Fig. 2 Comparison of calculated bending moment time histories with experimental data. r/R=.7; 1-12 harmonics

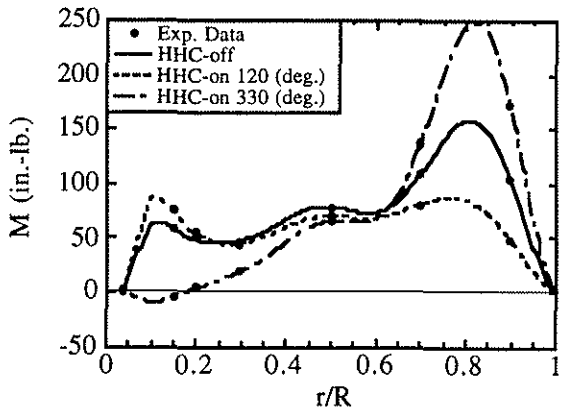

3(a1) 3rd harmonic - cosine term

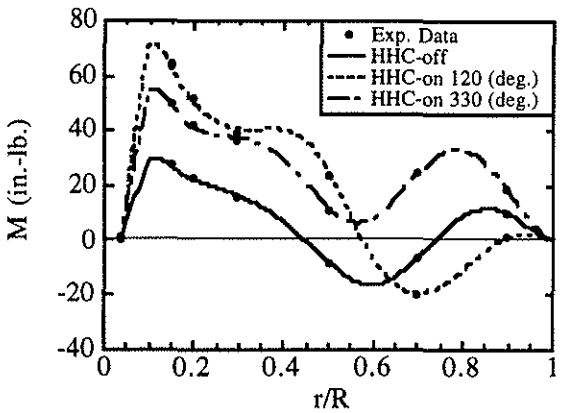

3(a2) 3rd harmonic - sine term

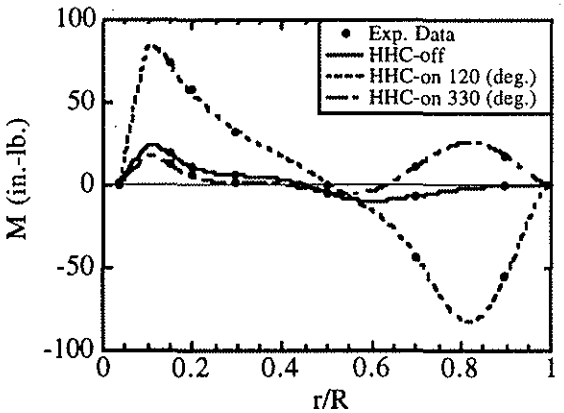

3(b1) 4th harmonic - cosine term

Fig. 3 Comparison of determined and calculated bending moment distribution with experimental data

be seen that the agreement between the experimental data, the determined and calculated results are also excellent.

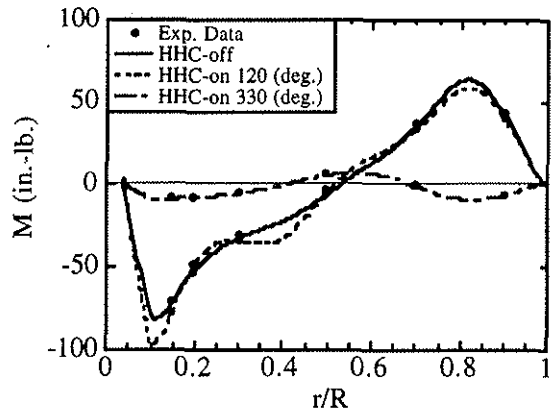

3(b2) 4th harmonic - sine term

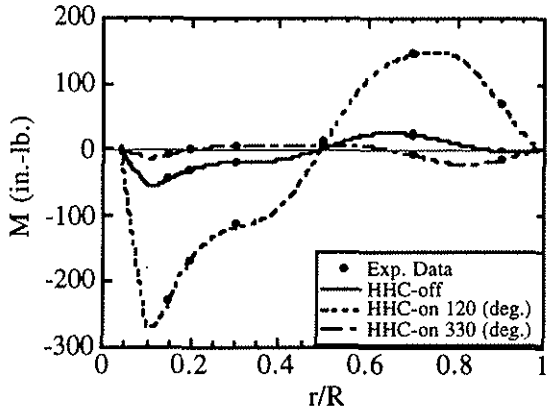

3(c1) 5th harmonic - cosine term

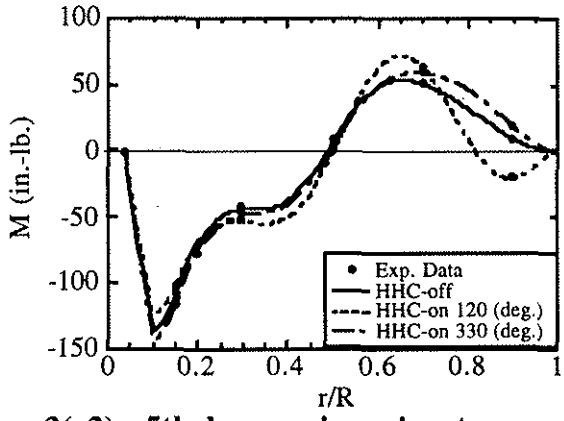

3(c2) 5th harmonic - sine term

Fig. 3 Comparison of determined and calculated bending moment distribution with experimental data

The above figures obviously have shown that the process of the displacement and load determination is correct, the ill-conditioned and underdetermined problems are avoided or solved and the SVD method is used successfully and can be quite useful in helping to insure that the correct solution is obtained. Furthermore, the iterative recurrence formula is valid and computationally efficient with the generalized coordinate converging to the solution in 3 to 4 iterations.

The total vibratory displacements, bending moments and airloads of the first 12 harmonics for the HHC-off (baseline), HHC-on 120 deg. and HHC-on 330 deg. cases are shown in Figures 4, 5, 6, 7, and 8, respectively.

In the above figures, the solid line represents the HHC-off case, the dashed line HHC-on 120 deg. and the dash-dot line HHC-on 330 deg.

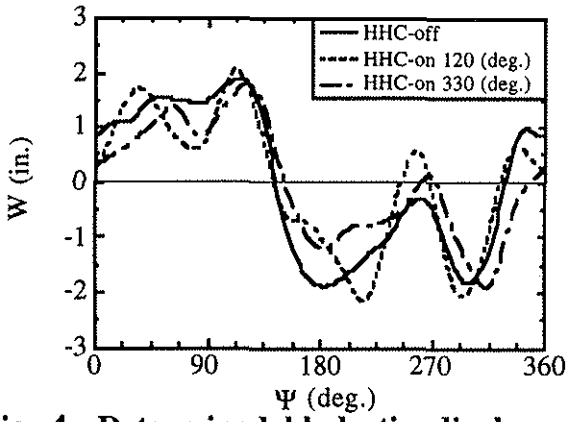

Fig. 4 Determined blade tip displacements; 1-12 harmonics

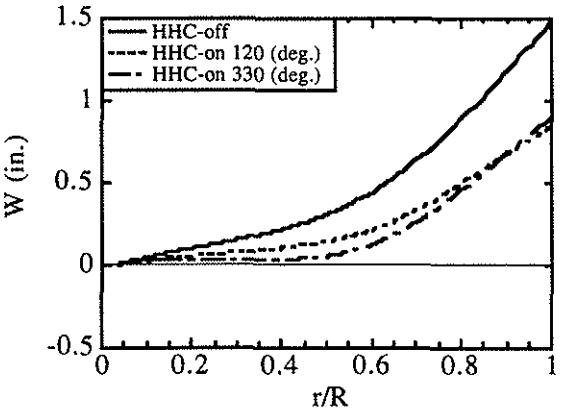

Fig. 5 Determined blade displacement distribution at 90 deg. azimuth; 1-12 harmonics

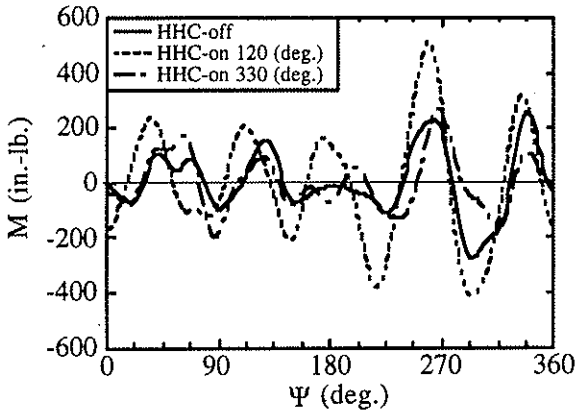

6(a) At r/R=0.15

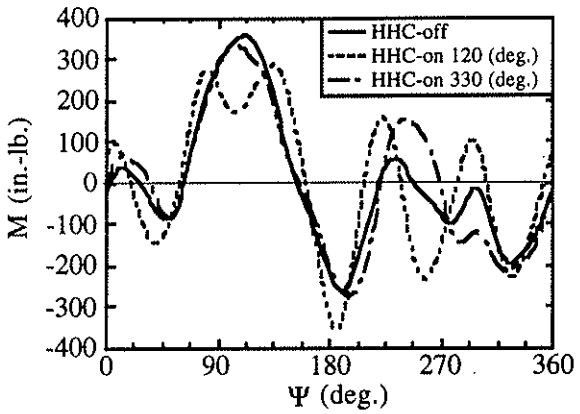

6(b) At r/R=0.7

Fig. 6 Determined blade bending moments; 1-12 harmonics

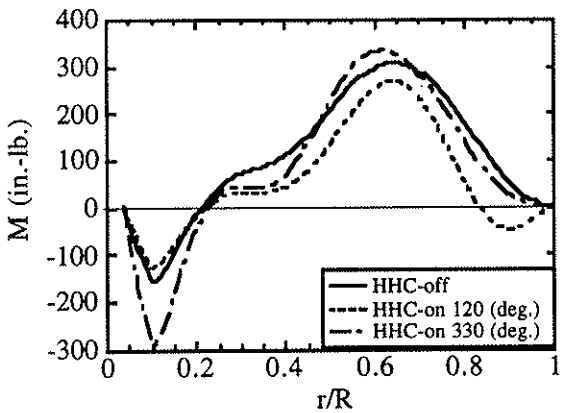

Fig. 7 Determined blade bending moment distribution at 90 deg. azimuth; 1-12 harmonics

Since only experimental bending moment data were available, the reasonableness of the determined airloads and displacements is also analyzed by checking the contributions of the

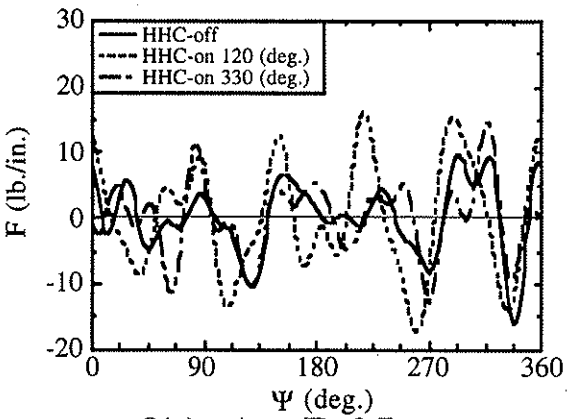

8(a) At r/R=0.7

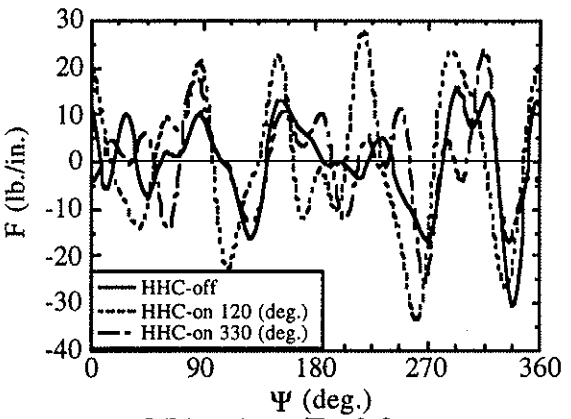

8(b) At r/R=0.9

Fig. 8 Determined blade airloads; 1-12 harmonics

airloads, inertia loads and centrifugal forces to the bending moment components for each harmonic and each mode. The conclusion is that the determined displacements and airloads shown in the above figures are, in general, reasonable. It is also considered that for the purpose of comparison between HHC-on and HHC-off, the difference among the three cases is more important than the accurate value.

The effect of HHC on blade displacements and airloads is analyzed as follows. Consider first Figure 4, which shows the variation of the blade tip flapwise displacements around the azimuth. It is observed that the maximum and minimum displacement value of the HHC-on 120 deg. case is larger than those of HHC-off and HHC-on 330 deg. cases. Also, for the HHC-on 330 deg. and HHC-off cases, both the maximum and minimum values are very close to each other and the maximum

displacement of HHC-on 330 deg. case is a little lower than that of the HHC-off case. This figure and the corresponding data also show that the main harmonic components of which the displacements consist are the first five harmonics. From the point of harmonic content, the difference between HHC-on 330 deg. case and HHC-off case is still small but in the HHC-on 120 deg. case, the 5th harmonic component is obviously increased. Figure 5 shows the blade flapwise displacement distribution along the radius at the 90 deg. azimuth. Combined with figure 4 and other related results, it is concluded that the displacements consist mainly of the first three modes. Also, the 1st mode displacement of the 1st harmonic component in the HHC-off case is larger than that of the HHC-on 120 and 330 deg. cases but the 1st mode displacement of the 5th harmonic component in the HHC-on 120 deg. is much more than that in the other two cases.

Shown in Figure 6 is the variation of the blade flapwise bending moments around the azimuth at r/R=0.15, and 0.7. At r/R=0.7, the difference of maximum and minimum value among the three cases is not large, but the 3rd harmonic component did show an increase in the HHC-on 330 deg. case and the 5th harmonic component showed an increase in the HHC-on 120 deg. case. At r/R=0.15, comparing with the baseline case, the difference is not large for HHC-on 330 deg. case but the effect of HHC-on 120 deg. is significant in which case the 5th harmonic component obviously increased. Referring to Figure 3 which show the 3rd, 4th and 5th harmonic components of the bending moment distribution along the radius, the same conclusion can be drawn. Furthermore, it is obvious that the 5th harmonic component in the HHC-on 120 deg. case is much higher than that in the other two cases from Figure 3(c). For the 4th harmonic component of the bending moment, Figure 3(b) shows clearly that comparing with the baseline, it is higher in the HHC-on 120 deg. case and it is lower in the HHC-on 330 deg. case. The bending moment distribution along the blade shown in Figures 3 and 7 indicates that the first four modes are main elements.

The blade airloads are shown in Figures 8(a) and (b). In these figures, the peak to peak airloads of the HHC-on 330 deg. case is close to those of the baseline case, but in the HHC-on 120 deg. case, the peak to peak airloads are obviously higher than those in either of the HHC-off or HHC-on 330 deg. cases. Comparing with the displacements (Figure 4), the higher harmonic components are much more important for the airloads, but the 5th harmonic component of the loads is still significant for the HHC-on 120 deg. case and is much higher than the other two cases. Combining the related data, it is indicated that the 4th harmonic component of the load in the HHC-on 330 deg. case is lower than that in HHC-off case, and it is higher in the HHC-on 120 deg. case.

It is interesting to note Figure 9. This figure shows the 4th harmonic component of the vertical forces at the flap hinge for the HHC-off, HHC-on 120 deg. and HHC-on 330 deg. cases. The line with arrow represents the total vertical force which is the summation of each modal contribution. The other line represents the individual modal contributions. The 1st mode vector starts from the origin of the coordinates. The other mode vectors follow in a successive manner. From the origin of the coordinates to the end of the last mode vector is the total vector of the vertical force.

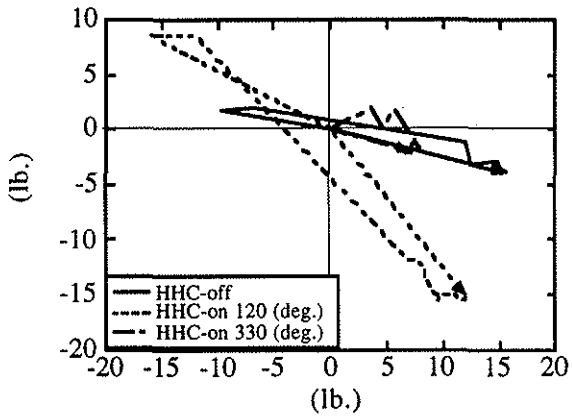

Fig. 9 4th harmonic component of the vertical forces at the flap hinge

Of significance, it can be seen that the 4th harmonic vertical force in the HHC-on 330 deg. case is much smaller than that in the HHC-off case and the vertical force in the HHC-120 deg. case is larger than the HHC-off case. Figure 9 also shows that in the baseline case (HHC-off), the 1st and 3rd modes are the main contributions, especially the 3rd mode. This is true for the HHC-on 120 deg. case as well, i.e. the 1st and 3rd modes are the main contributions and the 3rd mode vector is the largest, but both 1st and

3rd mode vectors in the HHC-on 120 deg. case are larger than those in the HHC-off case. Consequently, the total vertical force for the HHC-on 120 deg. case is larger than HHC-off. However, in contrast to the HHC-on 120 deg. case, the 1st and 3rd mode vectors in the HHC-on 330 deg. case are much smaller than the baseline case, especially the 3rd mode, so that the total vertical force in HHC-on 330 deg. case is much smaller than the HHC-off case.

The fact that the 4th harmonic component of the vertical force at the blade hinge is smaller in HHC-on 330 deg. case and larger in the HHC-on 120 deg. case is consistent with the vibration measurements taken during flight testing [4] and shown in Figure 10. In this figure are plotted the peak accelerations in g's as measured vertically and laterally by accelerometers mounted under the pilot's seat.

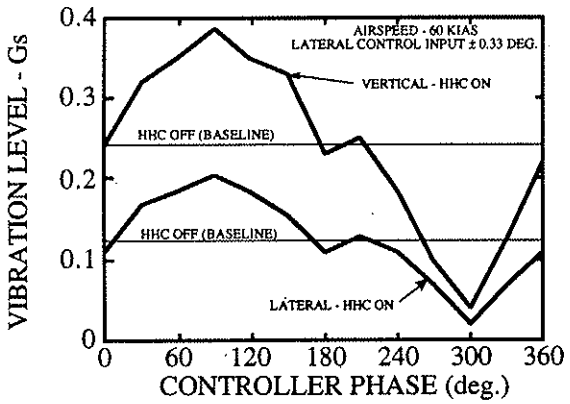

Fig. 10 Variation of 4th harmonic vibration with HHC input phase

In summary, the effects of HHC on blade displacements and loads, including structural loads and airloads, are consistent. For the total vibratory displacements and loads, the magnitudes in the HHC-on 330 deg. case are close to those in the baseline (HHC-off), while the magnitudes in the HHC-on 120 deg. case are obviously higher. It can be seen that the harmonic components of the vibratory forces due to HHC have been changed. The 5th harmonic component increased significantly in the HHC-on 120 deg. case. The 4th harmonic components of loads including bending moment, airload and vertical force at the flap hinge are higher in the HHC-120 deg. case and lower in the HHC-on 330 deg. case than those in HHC-off. For the higher 4th and 5th harmonic components in the HHC-on 120 deg. case, the 3rd modal contribution is the largest one. It should be mentioned here that the 3rd modal flap frequency of the light helicopter's rotor blade is about 4.88Ω.

The above analysis indicates that the high frequency blade pitch oscillations due to HHC causes changes to the rotor blade displacements and loads (structural loads and airloads) and hub loads. These changes, however, can induce vibrations which are better or worse than before HHC was applied, as evidenced in flight tests [4]. How it changes depends on the excitation input and the dynamic characteristics of the rotor blade, hub and control system. For a given helicopter, when the excitation mode, frequency and magnitude are fixed, the excitation input phase is very important. If the wrong phase angle is applied, HHC can serve to greatly increase the vibratory rotor loads and the vibration levels in the helicopter. In the cases analyzed, the effect of HHC-on 330 deg. is qualitatively good while the effect of HHC-on 120 deg. is bad. It should be emphasized that, based on the very limited amount of available data, it is impossible to comprehensively analyze the effect of HHC and furthermore this is not the intent of this paper.

Conclusions

1) The technique for rotor blade displacement and load determination has been applied using a flight test case of a light helicopter in forward flight with and without HHC. The process of determining blade displacement and loads (structural loads, airloads and hub loads) from measured blade bending moments is systematically described.

2) Some practical problems such as the ill-conditioned problem and the underdetermined problem could arise and have been investigated, analyzed and solved.

3) For calculation of the generalized coordinates, the SVD method is a powerful tool and has been, for the first time, applied successfully in the rotor blade displacement and load determination process to explore the ill-conditioned problem.

4) For the articulated rotor, it is necessary to use the measured flap angle in conjunction with an iterative process to determine the generalized coordinate of the first flapwise mode and a recurrence formula

in matrix form for this process has been developed.

5) The number of measured data points should not be less than the number of modes which are needed to fit the data. Otherwise, it is necessary to add some constraints in order to avoid the underdetermined problem.

6) The displacements and loads of the light helicopter rotor blade in three cases - HHC-off, HHC-on 120 deg. and HHC-on 330 deg. have been determined. The differences among them have been shown and analyzed. When the HHC excitation mode, frequency and magnitude are fixed, the excitation phase is very important. In the analyzed cases, the effect of HHC-on 330 deg. is qualitatively good for loads and vibration, while the effect of HHC-on 120 deg. is bad compared to the HHC-off case.

Acknowledgments

The authors wish to acknowledge Professor E. R. Wood, U. S. Naval Postgraduate School, Monterey, CA for his valuable comments during the analysis phase of this work.

References

1) McHugh, F.J., and Shaw, J., "Helicopter Vibration Reduction with Higher Harmonic Blade Pitch," Journal of the American Helicopter Society, Vol. 23, No. 4, October, 1978.
2) O'Leary, J., Kottapalli, S.B.R., and Davis, M.W., "Adaptation of a Modern Medium Helicopter (Sikorsky S-76) to Higher Harmonic Control," Rotorcraft Dynamics Conference, November, 1984.
3) Shaw, J., Albion, N., Hanker, E.J., and Teal, R.S., "Higher Harmonic Control: Wind Tunnel Demonstration of Fully Effective Vibratory Hub Force Suppression," Journal of the American Helicopter Society, Vol. 34, No. 1, January, 1989.
4) Wood, E.R., Powers, R.W., Cline, J.H., and Hammond, E.C., "On Developing and Flight Testing a Higher Harmonic Control System," Journal of the American Helicopter Society, January 1985.
5) Walsh, D.M., "Flight Tests of an Open Loop Higher Harmonic Control System on an S-76A Helicopter," Proceedings of the 42nd Annual Forum of the American Helicopter Society, Washington, D.C., 1986.
6) Miao, W.L., Kottapalli, S.B.R., and Frye, H.M., "Flight Demonstration of 76," Proceedings of the 42nd Annual Forum of the American Helicopter Society, Washington, D.C., 1986.
7) Polychroniadis, M., and Achache, M., "Higher Harmonic Control: Flight Tests of an Experimental System on SA 349 Research Gazelle," Proceedings of the 42nd Annual Forum of the American Helicopter Society, Washington, D.C., 1986.
8) Liu, ShouShen, and Davies, G.A.O., "The Determination of Rotor Blade Loading from Measured Strains," 13th European Rotorcraft Forum, 1987.
9) Liu, ShouShen and Li, Nanhui, "A Technique for Determining Rotor Blade Loads," Aerodynamic Experiment and Measurement and Control, Vol. 5, No. 2, June 1991.
10) Bousman, William G., "Estimation of Blade Airloads from Rotor Blade Bending Moments," 13th European Rotorcraft Forum, 1987.
11) Ory, H. and Lindert, H. W., "Reconstruction of Spanwise Airload Distribution on Rotor Blades from Structural Flight Test Data," 18th European Rotorcraft Forum, 1992.
12) Gaukroger, D.R. and Hassal, G.J.W., "Measurement of Vibratory Displacement of a Rotating Blade," Vertica, No. 2, 1978.
13) Tourjamsky, N. and Szechenyi, E., "The Measurement of Blade Deflections; a new implementation of the strain pattern analysis," 18th European Rotorcraft Forum, 1992.
14) Liu, ShouShen, Higman, Jerry and Schrage, Daniel, "On The Determination Of Helicopter Rotor Loads," American Helicopter Society Specialist Conference, San Francisco, California, January 19-21, 1994.
15) Leon, Steven j., Linear Algebra With Applications, Macmillan Publishing Co., Inc., New York, New York, 1980.